A 50 MW pulse-forming network with a voltage stability within 0.03%

B. J. H. Meddens, P. F. M. Delmee, and P. W. Van Amersfoort
FOM-Instituut voor Plasmafysica 'Rijnhuizen', Associatie EURATOM-FOM, Edisonbaan 14, 3439 MN Nieuwegein, The Netherlands

(Received 19 June 1992; accepted for publication 16 October 1992)

Requirements on electron energy stability are extremely tight for operation of a free-electron laser. In case a radio-frequency field is used to accelerate the electrons, this leads to stringent requirements on the stability of the klystron output power and, hence, on the stability of the source producing the cathode voltage. A pulse-forming network (PFN) capable of delivering a 19 kV pulse with a stability of 0.03%, during 20 μs, is presented. The PFN consists of four parallel lines, each containing 19 cells of a 20 nF capacitor and a 20 μH solenoid. The solenoids are equipped with taps and a plunge tuner. An innovative line switch is used, namely a stack of 32 thyristors in series. Numerical simulations of the pulse shape show that, in order to obtain the best possible pulse flatness, it is essential to arrange the capacitors such that the difference between adjacent capacitances is minimized.

I. INTRODUCTION

The free-electron laser (FEL) is a source of intense, coherent radiation, opening up many new applications.[1] In a FEL, a beam of relativistic electrons is injected into a spatially periodic magnetic-field structure, the so-called undulator or wiggler. This leads to a wiggling electron trajectory and, therefore, to the emission of radiation. The radiation is usually captured in an optical cavity and amplified on successive passes through the undulator. Part of the attractiveness of FELs lies in their tunability, which can be accomplished by variation of either the electron energy or the undulator field. This is shown by the FEL resonance condition,

$$\lambda_s=\frac{\lambda_u}{2\gamma^2}(1+K^2), \tag{1}$$

in which λ_s denotes the resonant wavelength, λ_u denotes the period of the undulator field, γ denotes the Lorentz factor the electrons (their energy divided by the rest energy), and K is a dimensionless parameter, which is proportional to the undulator field.

It is obvious from Eq. (1) that any fluctuation of the electron energy results in a fluctuation of the wavelength, which is undesirable for most FEL applications. In this respect it is important to note that the gain bandwidth is of the order of $1/2N$, where N denotes the number of undulator periods.[1] Since N is usually between 25 and 100 in order to achieve sufficient gain, the bandwidth is thus of the order of 1%. This implies that a shift of the electron energy of about 0.5% would cause the resonant wavelength to be shifted outside the gain bandwidth, so that the laser power has to build up again from noise. As an example of this highly undesirable situation we refer to an observation made at Los Alamos, where a sudden 0.6% drop in energy resulted in a decrease in output power of at least 70%.[2] This illustrates that requirements on energy stability are extremely tight for operation of a FEL. To satisfy the requirements is a difficult task, due to the high-electron-beam power, typically several tens of MW, and the long pulse length, preferably several tens of microseconds. The relatively long pulse is needed to produce a saturated laser output of sufficient duration. This article addresses an important aspect of stabilizing the electron energy in rf-linac-based FELs, namely the stabilization of the input voltage for the klystron that provides the rf power for the linac.

This paper is organized as follows. Elementary considerations leading to the requirement of a cathode voltage stability of at least 0.08% are discussed in Sec. II. The choice of a pulse-forming network-based modulator for production of the high-voltage pulse is explained in Sec. III. Numerical simulations of the pulse shape are presented in Sec. IV, and the technical layout of our modulator is discussed in Sec. V. Experimental results, which show that a better pulse flatness than the required value has been obtained, are presented in Sec. VI.

II. BASIC DESIGN CONSIDERATIONS

The work described in this article has been done in the context of the FELIX (free-electron laser for infrared experiments) project.[3] FELIX uses an accelerator consisting of a thermionic gun, a subharmonic prebuncher, a buncher, and two traveling-wave linacs. The electron beam can be bent into undulators behind each linac. The buncher employs the full output of a 20 MW klystron, which leads to an exit energy slightly below 4 MeV. The residual power at the buncher exit, approximately 18 MW, is used as input power for the linacs, after appropriate power division and phase adjustment.

The influence of a fluctuation of the rf power on the electron energy can be estimated as follows. The energy gain in each linac (in eV) is

$$T\approx\sqrt{[1-\exp(-2\tau)]RP_0L}-IRL\left(\frac{1}{2}-\frac{\tau}{\exp(2\tau)-1}\right), \tag{2}$$

where P_0 denotes the rf input power, R denotes the shunt impedance, L denotes the length of the accelerating structure, and τ denotes an attenuation parameter, which characterizes the rf structure.[4] The time-averaged beam current

 0034-6748/93/020568-09$06.00

TABLE I. Characteristic properties of the klystron used to generate the rf power for the buncher and the linacs. This klystron has been manufactured by Thomson-CSF (France) and is a slightly modified version of type TV 2002 DOD.

Frequency	2.9985 GHz
Cathode voltage	225 kV
Cathode current	203 A
rf input power	160 W
rf output power	20 MW
Pulse duration	25 μs
Perveance	1.83 $\mu A/V^{3/2}$
Efficiency	44%

is denoted as I. The first term on the right-hand side of Eq. (2) gives the energy gain in the absence of beam loading, and the second term gives the reduction due to beam loading. For the FELIX linacs, we have $R \approx 57$ MΩ/m, $L = 3.15$ m, $\tau \approx 0.41$, and, consequently, the energy gain is

$$T(\text{MeV}) \approx 10.0\sqrt{P_0}(\text{MW}) - 31.8I(\text{A}). \quad (3)$$

The maximum input power into each structure is around 8 MW, so that the maximum energy gain is 22 MeV at our beam current of 0.2 A. The minimum input power is 3 MW, which corresponds to an energy gain of 11 MeV. This way, the beam energy is 15–26 MeV behind the first linac, and 26–48 MeV behind the second linac.

It is clear from Eq. (3) that a fluctuation of either P_0 or I will cause a change in energy. Our objective is to stabilize the energy to within 0.1%, in order to stay well within the gain bandwidth. The achievable stability is determined mainly by the stability of P_0, in view of the fact that the beam loading term in Eq. (3), 6.4 MeV, is relatively small, in particular at the high-energy end of the operating range. This leads to the condition of a rf power stability better than 0.2%. Note that a fluctuation of the power on a time scale shorter than the filling time of the linacs (i.e., the length of the rf structure divided by the rf group velocity) is effectively damped by the structure, due to the high Q. The filling time of our linacs is of the order of 1 μs.

The klystron output power stability $\Delta P/P$ is related to the stability of the voltage applied to its cathode $\Delta U_c/U_c$ as[5]

$$\frac{\Delta P}{P} = \frac{5}{2}\frac{\Delta U_c}{U_c}. \quad (4)$$

Hence, a stability better than 0.08% is required for U_c. We are aware of the fact that the phase of the rf output also varies due to the varying cathode voltage, which causes electrons to be on different parts of the rf wave while traversing the linac.[5] This phase fluctuation is of the order of 0.5° at the desired cathode voltage stability of 0.08%.[6] The corresponding fluctuation of the electron energy is very small compared to the required stability of 0.1%.

III. THE PULSE-FORMING NETWORK

The specifications of the klystron that supplies the rf power for the buncher and the linacs are given in Table I.

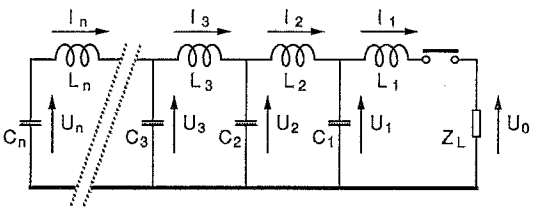

FIG. 1. Layout of a pulse-forming network consisting of N cells ($N = 19$ in our case). The sign convention for the currents and voltages used in model calculations of the pulse shape is indicated.

The required cathode voltage and current for this klystron, which has been manufactured by Thomson-CSF, are 225 kV and 203 A, respectively, and the corresponding power required from the high-voltage source is 46 MW. It is operated at a pulse duration of 25 μs, in order to obtain a flat top (during which the cathode voltage is stable within 0.08%) of 20 μs. The total energy required from the high-voltage source is thus of the order of 1150 J.

There are two customary approaches for production of a high-voltage pulse with these types of power specifications: a hard-tube modulator and a pulse-forming network. In the first approach a vacuum tube, usually a triode, is used to transfer the energy stored in a capacitor bank to the cathode of the klystron (see, for instance, Ref. 7). The droop of the voltage across the capacitors is compensated by application of an appropriately ramped signal to the grid. Naturally, the latter is only possible as long as the capacitor voltage is larger than the required cathode voltage. For our case, this would lead to a charging voltage of typically -350 kV. An obvious advantage of hard-tube modulators is the flexibility with which the pulse shape can be controlled. An obvious disadvantage is that only a fraction of the energy stored in the capacitors is used to generate rf power, of the order of 50%. Also, the high charging voltage would make the capacitors quite expensive, and would necessitate placing them in a tank filled with oil or SF_6. Another disadvantage is the dangerous overdose of stored energy, with no inherent limitation in case of a breakdown. In view of this, and in view of the extremely high cost of a 50 MW regulator tube, we have chosen the second approach, a pulse-forming network (PFN).

A PFN, as shown schematically in Fig. 1, is essentially a transmission line consisting of discrete capacitors and inductors. The characteristic impedance of the PFN is

$$Z_0 = \sqrt{L/C}, \quad (5)$$

where L and C denote the capacitance and inductance, respectively, of the components used (under the assumption that all capacitors and inductors are identical). The capacitors are charged to a voltage U_L with the load disconnected. The characteristic impedance is made equal to the impedance of the load, i.e., the impedance of the klystron "seen" through a pulse transformer, and, therefore, the voltage at the right-hand side of the PFN drops to $U_L/2$ when the load is connected. The subsequent discharging of the other capacitors can be represented by a wave front with an amplitude of $-U_L/2$ first traveling

TABLE II. Design parameters for the FELIX PFN.

Number of parallel lines	4
Number of cells per line	19
Nominal cell capacitance	20 nF
Nominal cell inductance	20 μH
Characteristic impedance	7.9 Ω
Charging voltage	38 kV
Stored energy	1.15 kJ
Output voltage	19 kV
Output current	2.6 kA
Output stability	0.08%
Pulse duration	25 μs
Flat top duration	20 μs
Repetition frequency	10 Hz

from the right- to the left-hand side (discharging all capacitors to $U_L/2$), then reflecting from the "open" left-hand-side end, and subsequently traveling from the left- to the right-hand side (discharging all capacitors to zero). The transit time of a pulse through a network made from N cells is approximately $N\sqrt{LC}$ s and, therefore, the output voltage pulse has amplitude $U_L/2$ and duration $2N\sqrt{LC}$.[8] The pulse shape can be tailored by adjustment of the capacitor and/or inductor values, as is discussed in Sec. IV.

An important advantage of a PFN modulator over a hard-tube modulator is that in a PFN modulator a relatively simple and inexpensive switch is used to transfer the stored energy to the klystron, instead of the regulator needed for a hard-tube modulator. Since switching elements for high currents are readily available, this permits the use of a reduced charging voltage and a step-up transformer behind the switching element. Another advantage is that the full energy stored in the capacitors is used to energize the klystron. A clear disadvantage is that the pulse shape is not controlled by an electronic signal, so that tailoring is more time consuming, and on-line correction during the pulse is impossible.

We have chosen a rather low charging voltage of 38 kV for the FELIX modulator, in order to be able to operate the PFN in (ambient) air. In view of the fact that the klystron voltage is 225 kV, the turns ratio required of the pulse transformer is 1:12. At the nominal cathode current of 203 A, the klystron impedance is 1110 Ω and, therefore, the load impedance for the PFN is 7.7 Ω. The required pulse duration of 25 μs is achieved by choosing the characteristic properties of the PFN as follows: $C=20$ nF, $L=20$ μH, $N=19$. The 20th capacitor has two times the nominal value, so that only 18 inductors are needed. The corresponding line impedance is 32 Ω and, consequently, four parallel lines are needed to match the PFN to the load. The total energy stored in the capacitors is then equal to the required value, 1150 J. The design parameters are summarized in Table II.

It is important to note that in choosing these design parameters we are deviating from the frequently used rule of thumb that a high-quality PFN should have typically three cells for each microsecond of pulse duration.[9] According to this, 60 cells would be required for FELIX. However, in Sec. IV we show, using a numerical model of the PFN discharging process, that a pulse flatness better than the required 0.08% can be obtained with our design parameters. More important, this is confirmed by the experimental results presented in Sec. VI.

IV. SIMULATIONS OF THE PULSE FLATNESS

An elementary circuit analysis of the network in Fig. 1 shows that the voltages and currents in the PFN, after it has been connected to the load, are governed by the differential equations

$$L_n \frac{\partial I_n}{\partial t} = U_n - U_{n-1}, \tag{6}$$

$$C_n \frac{\partial U_n}{\partial t} = I_{n+1} - I_n, \tag{7}$$

with $I_{N+1}=0$. Together with the boundary condition for the first cell, $U_0=Z_L I_1$, these are $2N+1$ coupled differential equations for $2N+1$ variables, U_0-U_N and I_1-I_N. The initial conditions at $t=0$ are: $U_0=0$, $U_n=U_L$ (for $n\geqslant 1$), $I_n=0$ (for all n). For a discrete time interval Δt, these differential equations lead to the difference equations

$$\Delta I_n = \frac{U_n - U_{n-1}}{L_n}\Delta t, \tag{8}$$

$$\Delta U_n = \frac{I_{n+1} - I_n}{C_n}\Delta t. \tag{9}$$

With these equations, the change of the voltage and the current in each cell during the interval Δt could, in principle, be calculated using the values of I_n and U_n obtained after the previous time step as input parameters. However, in using Eq. (8) to calculate the currents this would involve the assumption that the capacitor voltages are constant, whereas in reality the drop during the investigated time interval, and vice versa for Eq. (9). The errors associated with this can be made small by choosing a sufficiently small time step, but this imposes quite excessive demands on computer time. Also, this approach has the inherent disadvantage that errors essentially add up in successive cells and time steps. For this reason we have chosen a different approach, which is based upon the condition that the time steps are sufficiently short to assume the change of the voltages and currents to be linear in time. Hence, in Eq. (8) U_n can be replaced by $U_n+\Delta U_n/2$, where U_n is the capacitor voltage obtained after the previous time step and ΔU_n is the change of the voltage during the interval under consideration. With a similar approximation for U_{n-1}, I_{n+1}, and I_n, this leads to the set of difference equations

$$\Delta I_n \approx \frac{U_n - U_{n-1}}{L_n}\Delta t + \frac{\Delta U_n - \Delta U_{n-1}}{2L_n}\Delta t, \tag{10}$$

$$\Delta U_n \approx \frac{I_{n+1} - I_n}{C_n}\Delta t + \frac{\Delta I_{n+1} - \Delta I_n}{2C_n}\Delta t, \tag{11}$$

which can be solved using the following iteration procedure. In the first calculation of a given time slice, the lists

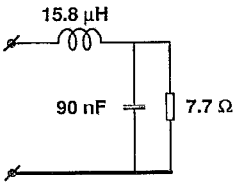

FIG. 2. Assumed load impedance. The klystron impedance is 7.7 Ω at the primary side of the pulse transformer. The capacitor represents the measured stray capacitance of the pulse transformer and the klystron. The solenoid represents the residual inductance of a switch plus the stray inductance of the pulse transformer.

of U_n and I_n obtained after the previous time slice are used as input parameters for Eqs. (10) and (11), neglecting the second terms (which are a small correction) on the right-hand side. This leads to a first-order estimate of ΔU_n and ΔI_n for each cell. In the next iteration step, these estimates are used to calculate the correction terms, which leads to a second-order estimate of each ΔU_n and ΔI_n. This iteration process is continued until the results are stable within a specified value, and subsequently, the next time slice is addressed, until the PFN has been fully discharged. The shape of the output pulse is kept track of via the relation $U_0 = Z_L I_1$.

In order to speed up the calculation, we decided to use the values for ΔU_n and ΔI_n that were obtained in the previous time slice as start values for calculating the correction terms in the first iteration step of the next time slice. This is based upon the expectation that, in a properly designed PFN, the changes in voltage and current are quite similar in each time slice, except at the start and at the end of the pulse. Using this strategy we found that, for a time slice of the order of 0.002 times the total pulse duration, the voltages and currents are stable within 0.001% in typically three iteration steps. This small number permits us to do our calculations on a simple personal computer. A complete calculation of (a single line of) the PFN then takes approximately 3 min.

In our model calculations we represent the PFN by a single line of 19 cells, with nominal capacitor and inductor values of 80 nF and 5 μH, respectively. The assumed load impedance is shown in Fig. 2. The capacitor represents the stray capacitance of the pulse transformer and the klystron. The inductor represents the stray inductance of the pulse transformer plus the residual inductance of a saturable inductor that is used for thyristor protection (see Sec. V C). This complex impedance makes it more difficult to properly match the PFN to the load than for the "ideal" situation in Fig. 1; however, it has the advantage that a ripple on the output voltage is attenuated, because the extra capacitance and inductance form a filter.

In our first model calculation, all capacitors of the PFN were assumed to have the nominal value. The pulse form obtained when all inductors are also set at the nominal value is shown in Fig. 3(a). As expected, there is a strong transient at the start of the pulse, due to the fact that the PFN is not matched to the complex load impedance in this case. There is also a transient at the end of the

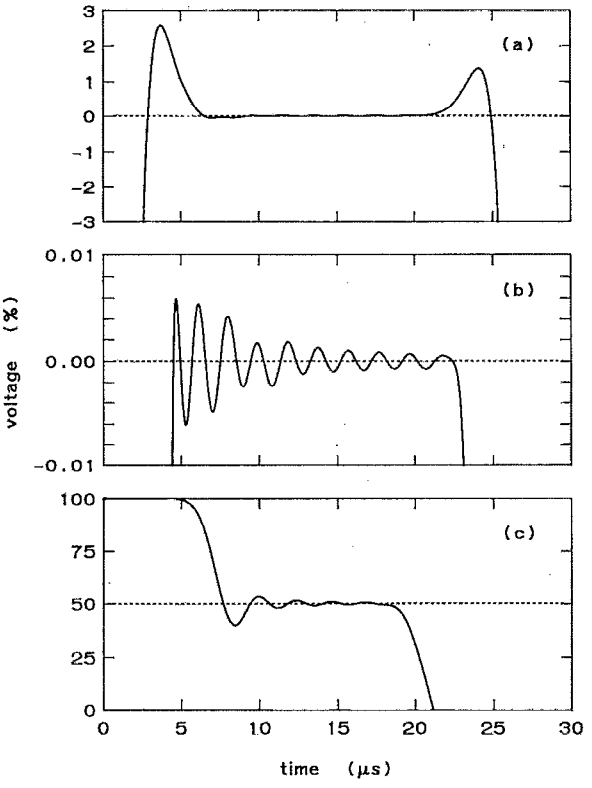

FIG. 3. Simulated top of the output pulse for an ideal PFN (i.e., for the case that all C_n have the nominal value) consisting of a single line, showing the fractional deviation from the nominal voltage. (a) The case that all L_n are set at their nominal value; (b) the top of the pulse for an optimized distribution of inductances. This distribution is given in Fig. 4(a). The stability is of the order of 0.01% during 20 μs. (c) The voltage across C_{10} is shown for the optimized case.

pulse because the last capacitor has two times the nominal value.

The following procedure is used for optimization of the pulse flatness. By trial and error, the inductors at the front and at the end of the line, L_1–L_3 and L_{16}–L_{18}, are adjusted to reduce the "shoulders" of the pulse. The subsequent optimization of L_4–L_{15} is performed by the computer. The program first determines the deviation from the intended voltage (half the charging voltage) at the times when the wavefront passes L_4–L_{15} and C_4–C_{15} in the PFN. In order to improve the stability of the procedure, this deviation is calculated as the sum of the value at the component in question and 50% of the deviations at the two adjacent components. The voltage deviation thus found at the times corresponding to L_4–L_{15} is compensated by changing these inductances by 0.15% for each percent of deviation. The deviation at the times corresponding to C_4–C_{15} is subsequently compensated by changing the two adjacent inductance values by 0.1% for each percent. This procedure is repeated until a specified pulse flatness has been obtained. For our required pulse flatness, the entire procedure takes typically 2 h on a simple personal computer.

The pulse shape for a thus-optimized PFN with nominal capacitances is shown in Fig. 3(b), and the corresponding distribution of L_n is given in Fig. 4(a). It is seen that a pulse flatness of the order of 0.01% is obtained,

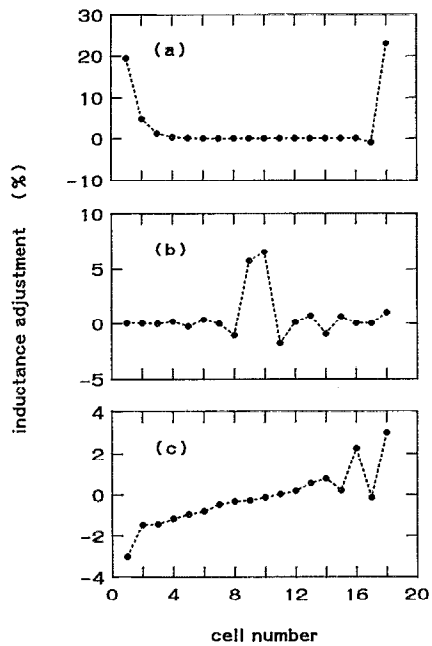

FIG. 4. (a) Distribution of inductances needed for optimization of the pulse flatness in the case that all C_n have the nominal value. (b) The correction required in case C_{10} is 10% larger than the nominal value. (c) The correction required for the distribution of C_{10} in Fig. 6.

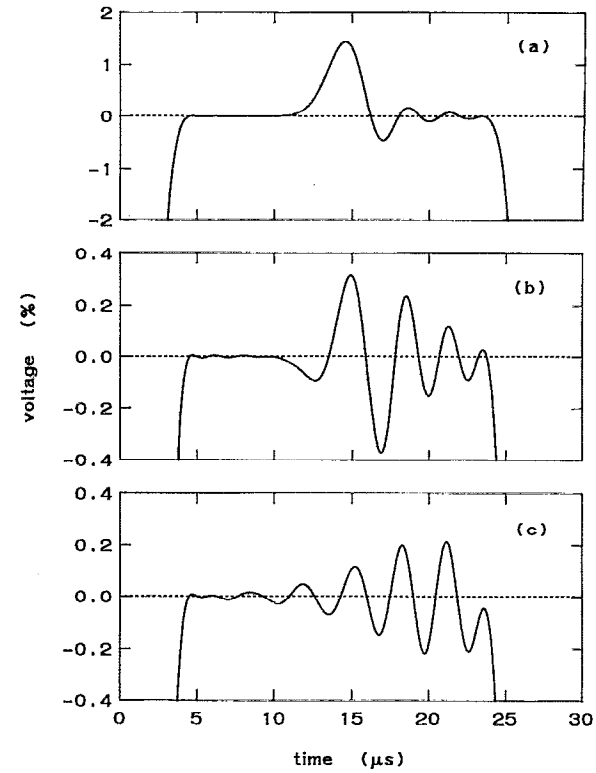

FIG. 5. Simulated top of the output pulse for a PFN consisting of a single line in which C_{10} is 10% larger than the nominal value. (a) The case that all L_n are set at the values optimum for an ideal PFN. (b) The top of the pulse in case the inductors adjacent to C_{10} are adjusted for nominal impedance of this cell. (c) The top of the pulse for an optimized distribution of inductances. This distribution is given in Fig. 4(b). The stability is of the order of 0.4% during 20 μs.

which is well within the design value of 0.08%. The inductances differ from their nominal values mainly in cells 1–3 and 17 and 18.

The next step is to investigate the influence of an imperfection in the PFN. We assume that the tenth capacitor has a capacitance 10% larger than the nominal value, i.e., $C_{10}=88$ nF. The resulting pulse shape is shown in Fig. 5(a). Obviously, the imperfection leads to a distortion of the pulse shape, which is most pronounced 14.5 μs after the start of the pulse. This can be understood straightforwardly: The wave front discharging the PFN reaches the tenth cell approximately 6.3 μs after the start of the pulse, and the different characteristic impedance in this cell leads to a reflection of part of the pulse, which reaches the load impedance 6.3 μs later. In addition, the complex load impedance leads to a delay of 2 μs.

The result in Fig. 5(b) is obtained after the characteristic impedance of the tenth cell has been made equal to the nominal impedance by adjustment of its inductance. This leads to a voltage stability of the order of 0.7%. Application of our optimalization procedure leads to a somewhat better stability of 0.4% [see Fig. 5(c)], which is roughly a factor of 40 worse than for the optimized "ideal" PFN of Fig. 3(b). The change in inductance values required for this [relative to those in Fig. 4(a)] is given in Fig. 4(b). It is seen that mainly the inductances adjacent to the tenth capacitor have been readjusted.

The degradation of the achievable pulse flatness can be understood as follows. The cell impedance scales with $\sqrt{L_n/C_n}$, whereas the propagation time scales with $\sqrt{L_nC_n}$, so that it is impossible to obtain simultaneously the nominal impedance and the nominal propagation time in each cell by trimming of its inductors. The wave front traveling through the PFN induces a (damped) oscillation in each cell. This is illustrated in Fig. 3(c), where we show the voltage across C_{10} for an ideal PFN. If the propagation time is identical in each cell, the oscillations induced in adjacent cells have a fixed phase difference at the load, with the consequence that they effectively cancel out. However, in case a cell has a different propagation time, the phase of the induced oscillation is different, so that complete cancellation is impossible. This view is corroborated by the observation that the oscillation of the output voltage in Fig. 5(a) is quite similar to the oscillation of the voltage across C_{10} in Fig. 3(c).

In existing PFNs, the capacitors are usually mounted more or less at random, i.e., without any specific strategy as regards their deviation from the nominal value, the idea being that irregularities in the output voltage can be eliminated by trimming of the inductors. The resulting poor pulse flatness may have generated the widespread idea that a stability better than a few tenths of a percent cannot be achieved, and the frequently used rule of thumb that a minimum of three cells should be used for each μs of pulse duration.[8]

We expect an improved performance when the capacitors are arranged in such a way that the difference in propagation time of adjacent cells is minimized, i.e., when

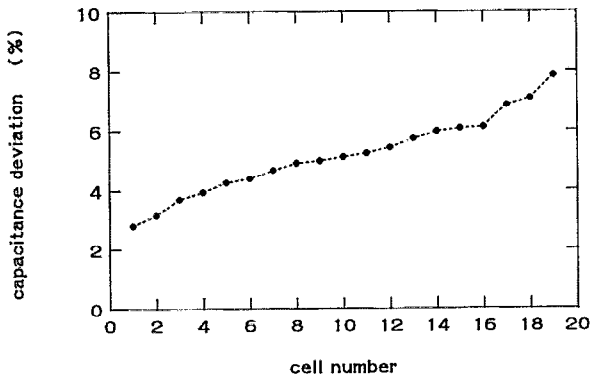

FIG. 6. Distribution of capacitances used in (one of the lines of) the FELIX PFN. The fractional deviation from the nominal value (20 nF) is shown.

adjacent capacitors have almost equal values. The distribution used in (one of the lines of) the FELIX PFN, where the capacitances deviate from the nominal value by 2.6%–8%, is shown in Fig. 6. The capacitors are arranged such that the largest capacitance is at the end of the PFN, and the smallest capacitance is closest to the load. The optimized pulse shape is shown in Fig. 7 and the corresponding L_n are given in Fig. 4(c). The achieved stability is seen to be of the order of 0.02%. This stability is only a factor of 2 worse than the stability of the optimized "ideal" PFN in Fig. 3(b), even though our PFN has only 0.8 cells per μs of pulse duration.

V. TECHNICAL SETUP

Our klystron modulator, which is shown schematically in Fig. 8, consists of four modules: (1) the PFN charger; (2) the PFN with associated circuits; (3) the line switch; (4) the pulse transformer and the klystron. The last module is partly immersed in an oil tank. The others are operated in air, in order to facilitate maintenance.

A. The PFN charger

Two power supplies are used in parallel to charge the PFN to a positive voltage of 38 kV. The first is a high-efficiency switching converter unit (manufactured by FUG, Germany) which has been designed especially for capacitor charging purposes. The maximum output voltage

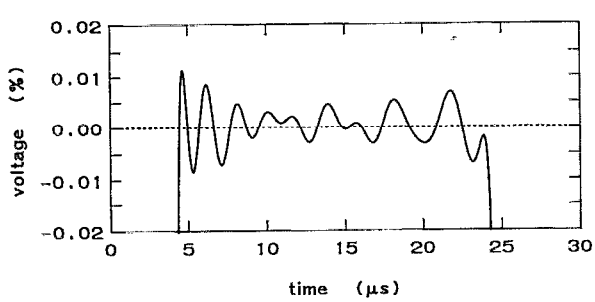

FIG. 7. Result of a simulation showing the top of the pulse for the FELIX PFN (represented by a single line), for the distribution of capacitances shown in Fig. 6 and the distribution of inductances shown in Fig. 4(c). The stability is of the order of 0.02% during 20 μs.

of this unit is 40 kV and it has a voltage precision of the order of 0.01%. Its maximum current is 400 mA, so that the PFN can be charged to the operating voltage in approximately 160 ms. Hence, the maximum repetition rate that can be achieved with the FUG unit is around 6.5 Hz. A second, unstabilized power supply (a variable three-phase transformer and a rectifier) has been installed to deliver the additional current needed for 10 Hz operation. The maximum output voltage of this supply is above 40 kV and its output current is limited to 400 mA by means of 20 mH inductors in the 50 Hz power input. This second power supply is set at a maximum voltage of 37 kV. The charging voltage precision is maintained by the FUG unit.

B. The PFN

The PFN consists of four parallel lines, each containing 19 cells. The nominal capacitor and inductor values are 20 nF and 20 μH, respectively. The low-inductance pulse capacitors (CSI, type 60N4685) consist of stacked paper and polycarbonate foil, immersed in oil. Their maximum dc hold-off voltage is 60 kV. The coils consist of solid copper wire with a diameter of 4.5 mm, which is wound on a grooved glass-fiber-epoxy bobbin with a diameter of 150 mm (see Fig. 9). Each coil is equipped with a tap for coarse adjustment and a plunger for fine tuning. The number of turns is 19, over a coil length of 220 mm, but 15 turns are normally used. Adjustment of the tap permits variation of the inductance by about 8%, while the fine adjustment has a span of 16% for a plunger scan of 100 mm. The capacitors and coils are placed on a grounded metal support plate. The plungers can be adjusted manually by means of threaded glass-fiber-epoxy rods penetrating through the support plate. This permits tuning of the PFN at the full charging voltage.

A fast crowbar is used to discharge the PFN in case of an emergency. The crowbar switch is an ignitron, which is fired when arcing occurs in the oil tank or in the klystron. The latter is detected by monitoring the klystron voltage with a capacitive voltage divider and a differentiator. Note that the normal rise and fall time of the pulse is of the order of 3 μs, while it will be far smaller in case of a breakdown.

It has been discussed in Sec. III that for maximum energy transfer, the impedance of the load (the pulse transformer and the klystron) should be equal to the characteristic PFN impedance. However, in practice there must be a certain misadjustment, in order to open the line switch (a thyristor stack; see Sec. V C) after discharging the PFN. Due to this misadjustment, and due to the use of discrete components instead of a continuous transmission line, the voltage at the end of the line does not drop to zero when the discharging "wave front" reaches this position, but can easily become several kV negative. This effect will be even stronger when there is a breakdown in the PFN or in the load, or when the fast crowbar is activated. The negative voltage could severely damage the power supplies and, after traversing the PFN, would lead to a positive voltage at the klystron that could damage the cathode. Note that, according to the klystron manufacturer, the cathode volt-

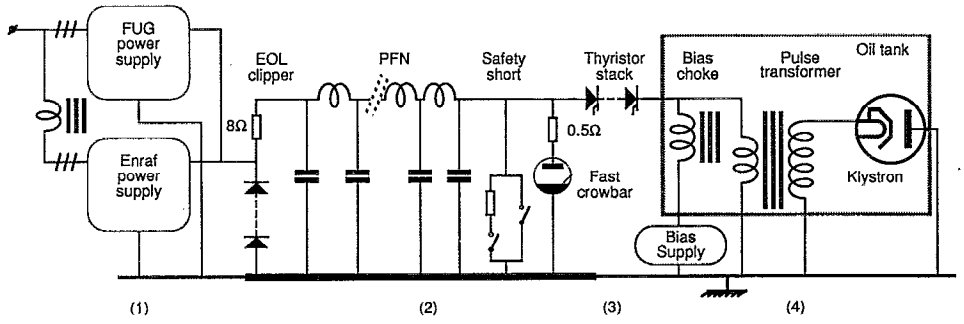

FIG. 8. Simplified layout of the FELIX modulator, which consists of four modules: (1) the PFN charger, (2) the PFN with associated circuits, (3) the line switch, (4) the pulse transformer and the klystron. For simplicity, only one of the four lines forming the PFN is shown.

age should not exceed 50 kV positive. Therefore, adequate damping, so-called end-of-line clipping, is necessary. Our end-of-line clipper consists of a stack of 12 diodes in series with a resistor of about the same value as the characteristic line impedance (8 Ω). Hence, when the voltage at the end of the PFN reverses polarity, the diodes become conductive and most of the pulse energy is dissipated in the resistor. Protection of the power supplies is provided by the fact that these units are connected to the PFN at the point between the resistor and the diodes, so that the (negative) voltage at this point cannot exceed 50 V. The diodes are ABB-type DSA405-50A. This type has been chosen because it can withstand a peak current of 3.5 kA with a rise time of 1.5 μs, which is the expected current in case of crowbar activation.

C. The line switch

In existing PFNs, hydrogen thyratrons are frequently used as the switching element. The voltage drop across these tubes lies between 100 and 250 V. If this voltage would vary by a quite reasonable amount of, say, 20 V during a 20 μs pulse, it would induce an uncertainty of 0.1% in the output voltage, which is unacceptable for our application. For this reason, we have chosen the innovative approach of using a stack of 32 reverse-conducting thyristors (ABB, type CSR331-20) as line switch. The total hold-off voltage of the 32 thryristors in series is 57 kV. Each thyristor has its own gate transformer circuit and also a punch-through-voltage protection circuit with "breakover diodes." The gate pulse generator has a number of built-in control circuits to ensure that the gate current pulses are sufficiently high, since too low pulses would cause thyristor damage. A saturable inductor has been placed between the thyristors and the pulse transformer in order to protect the thyristors against the large dI/dt values that otherwise would develop in case of a breakdown. This inductor blocks the 38 kV voltage during 0.6 μs after firing the thyristors. The magnetizing current is 100 A. After 0.6 μs, the thyristor conductivity has become sufficiently large to withstand a breakdown. The residual inductance after saturation of the ferrite core is 6 μH. The design and performance of the line switch will be discussed in detail in a future paper.

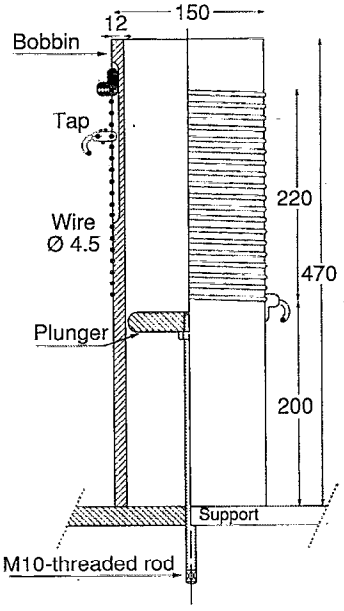

FIG. 9. Schematic view of the solenoids used in our PFN. The bobbin on which the copper coil is wound is made from glass-fiber epoxy. The plunger is made from aluminum, and the threaded rod with which the plunger can be positioned is made from glass-fiber epoxy. This way, the plunger is at the same potential as the coil, which was found necessary to reduce "corona" discharges between these parts. Dimensions are in mm.

D. The clipper amplifier

A dummy load was used as the terminating element in measurements of the achievable pulse flatness (see Sec. VI). In order to see voltage fluctuations well within 0.1% of the 1 V pulse derived from this load (via a voltage divider), we have developed a differential amplifier with offset control. The offset range is ±1.5 V. The output voltage is clipped at −1 V in between successive pulses, because otherwise it would saturate after the end of a pulse, and would not have recovered before the start of the next pulse. The main problem in designing the clipper amplifier was that it must simultaneously fulfill the requirement of a gain of a factor of 10 (in order to obtain an output voltage of 10 mV for 0.1% fluctuation of the PFN pulse) and a bandwidth of 3 MHz (in order to see fluctuations well within 0.1 μs). In addition, amplifier operation must be stable in two different gain regimes. At low gain (clipping) the closed loop compensation must be large enough to avoid oscillations, but this limits the bandwidth at high

gain (amplification of the top of the pulse). We use a cascade of two commercially available clipping amplifiers with a gain-bandwidth product of 10 MHz (type CLC 501, Comlinear Corporation), each adjusted for $\sqrt{10}$ gain. In between successive PFN pulses, their output voltage is clamped at $+1$ and -1 V, respectively. The noise level at the output is about 1 mV. This permits the observation of 0.01% fluctuations in the PFN pulse.

VI. RESULTS

We have adjusted the PFN in three steps, using a dummy load as the terminating element. The first step, which was done at a low charging voltage of 25 V, is to optimize the pulse flatness and to adjust the characteristic impedance of each of the four lines separately. The second step is to connect the four lines in parallel and to check the pulse flatness. This step was also done at a charging voltage of 25 V. The third step was done at the nominal charging voltage (38 kV), using the thyristor stack to switch the dummy load on. The dummy load for the second and third step is shown in Fig. 2. The resistor, capacitor and inductor values for the first step were changed to 30.8 Ω, 22.5 nF, and 63.2 μH, respectively. Simple low-voltage components were used in the first two steps.

In the first step, with all coil taps and plungers initially in the same position, we adjusted the plungers (and, if necessary, the taps) to obtain a pulse flatness within 1%, following a procedure similar to that in the numerical simulations. At the same time, the duration of the flat top was kept as long as possible. After this, we fine tuned all coils by the same amount in order to obtain a matched impedance. This was done by looking at the voltage level, keeping in mind that some mismatch is necessary (there must be a small negative reflection at the end of the pulse to allow the thyristors to cease conducting). Subsequently, each coil was readjusted separately to obtain the best possible pulse flatness. After this procedure had been carried out for each of the four lines individually, we connected them in parallel. The resulting pulse shape at the full charging voltage of 38 kV is presented in Fig. 10. The upper trace gives the full pulse (with 450 mV per division along the vertical axis) and the lower trace gives the top of the pulse (0.5 mV per division). For the latter trace, one division along the vertical axis thus corresponds to 0.11% of the peak voltage. It is seen that the achieved stability is within 0.03% during 20 μs. This is consistent with the value obtained from the simulations, 0.02%.

The achieved stability is typically an order of magnitude better than the stability obtained with other state-of-the-art klystron modulators. For instance, we estimate the stability of the 350 kV voltage pulses produced at the Stanford Linear Collider, as shown in Ref. 10, to be of the order of 0.3% during 4 μs.

Finally, the following remark is in order. We are aware of the fact that the pulse transformer used to increase the PFN output voltage to the required klystron cathode voltage introduces a sizeable droop, due to core magnetization and loss. This droop can be compensated by providing a slightly ramped PFN output voltage. Our simulations have shown that, for the chosen distribution of C_n (see Fig. 6), a ramp with a similar small deviation from an ideal ramp as the achieved flat top stability can be produced, by straightforward trimming of the inductors. A discussion of the achieved stability of the klystron output power (which has been found to be well within 0.1% during 20 μs) and the type of ramp used for this is the subject of a future paper.

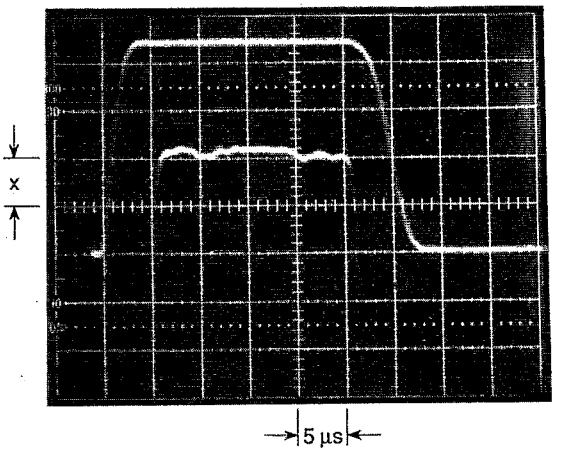

FIG. 10. Experimentally obtained pulse shape at the full PFN charging voltage (38 kV): full signal (upper trace, $x=450$ mV) and detailed view of the top (lower trace, $x=0.5$ mV). For the lower trace, a division along the vertical axis corresponds to 0.11% of the pulse height. The achieved stability is within 0.03%, during 20 μs.

ACKNOWLEDGMENTS

The advice of E. Heine and F. B. Kroes (NIKHEF-K, Amsterdam), C. R. Dunbar and J. B. Lyall (SERC Daresbury Laboratory, Daresbury), and M. G. Kelliher (Kelvin Laboratory, Glasgow) in designing our modulator has been indispensable and is gratefully acknowledged. We are indebted to A. M. van Ingen and A. B. Sterk of our Institute for valuable discussions and assistance. This work has been performed as part of the research program of the association agreement between the Stichting voor Fundamenteel Onderzoek der Materie (FOM) and EURATOM, with financial support from the Nederlandse Organisatie voor Wetenschappelijk Onderzoek (NWO) and EURATOM.

[1] T. C. Marshall, *Free Electron Lasers* (Macmillan, New York, 1985).
[2] W. E. Stein, W. J. D. Johnson, J. F. Power, and T. J. Russel, Nucl. Instrum. Methods A **296**, 697 (1990).
[3] P. W. van Amersfoort, R. J. Bakker, J. B. Bekkers, R. W. B. Best, R. van Buuren, P. F. M. Delmee, B. Faatz, C. A. J. van der Geer, P. Hellingman, D. A. Jaroszynski, P. Manintveld, W. J. Mastop, B. J. H. Meddens, A. F. G. van der Meer, J. P. Nijman, D. Oepts, J. Pluygers, W. Wang, and M. J. van der Wiel, Nucl. Instrum. Methods A **304**, 163 (1991).
[4] J. E. Leiss, in *Particle Accelerators*, edited by P. M. Lapostolle and A. L. Septier (North-Holland, Amsterdam, 1970), pp. 147–172.
[5] J. Haimson, in *Particle Accelerators*, edited by P. M. Lapostolle and A. L. Septier (North-Holland, Amsterdam, 1970), pp. 415–470.
[6] P. W. van Amersfoort, R. W. B. Best, C. A. J. van der Geer, W. J. Mastop, B. J. H. Meddens, A. F. G. van der Meer, and D. Oepts, The

FELIX Project, Status Report, April 1988, Rijnhuizen Report 88-176, Nieuwegein, 1988.
[7] W. J. D. Johnson, M. T. Lynch, P. J. Tallerico, D. R. Keffeler, and J. O. Hornkohl, Nucl. Instrum. Methods A **272**, 232 (1988).
[8] S. Humphries, *Principles of Charged Particle Acceleration* (Wiley, New York, 1986), pp. 240–258.
[9] Private communication at the 18th Power Modulator Symposium, Hilton Head, SC, June 20–22, 1988.
[10] M. A. Allen, W. R. Fowkes, R. F. Koontz, H. D. Schwarz, J. T. Seeman, and A. E. Vlieks, in Proceedings of the 1987 IEEE Particle Accelerator Conference, March 16–19, 1987, Washington DC, edited by E. R. Lindstrom and L. S. Taylor, pp. 1713–1715.